preprint, finally published in European Journal of Mechanics B/Fluids ***23*** *(2004), 835-849*

Control of Separated Flows by Time Periodic Lorentz Forces

T. Weier*, G. Gerbeth

Forschungszentrum Rossendorf, P.O.Box 51 01 19, 01314 Dresden, Germany

Abstract

Electromagnetic, i.e. Lorentz forces, may be used to influence the flow of electrically conducting fluids. The present paper investigates the application of time periodic Lorentz forces to the control of the suction side flow on a NACA 0015 hydrofoil. Experimental results, consisting of flow visualizations and force measurements, characterizing the control effect in the low Reynolds number range of $10^4 \lesssim Re \lesssim 10^5$, are presented. A comparison of the forcing effect with stationary Lorentz forces on one hand and conventional oscillatory blowing on the other hand is given as well.

Key words: **electromagnetic flow control/separation control/periodic excitation**

1 Introduction

Control of flow separation is a persistent topic of fluid dynamic research because of its relevance to practical applications. Usually, flow separation implies a loss of lift, an increase of drag, diminished pressure recovery, etc. Extensive reviews of the earlier research on separation control can be found in [1] and [2]. More recent results are discussed, e.g., in [3]. Aside from passive means, like shaping and deployment of vortex generators, active methods reviewed in the references cited above are mostly limited to the steady supply of momentum to the near wall flow. This could, e.g., be achieved by blowing, suction, or wall motion. Only in the last two decades periodic addition of momentum, mostly realized through oscillatory blowing and suction, has become a subject of intensive research. Meanwhile, periodic excitation has proven to be a valuable tool to control flow separation. A thorough review can be found in

Email address: T.Weier@fz-rossendorf.de, *Tel.:* +49 351 260 2226, *Fax:* +49 351 260 2007 (T. Weier).

[4]. Experimental and numerical results on this type of separation control give strong evidence that key features are related to the dynamics of perturbed shear layers. Most appealing with respect to practical applications is the reduction of the control effort by about two orders of magnitude compared to steady actuation (see e.g. [5]).

If the fluid is electrically conducting, an electromagnetic body force can be generated by the application of magnetic and/or electric fields. Flows of such kind are the topic of Magnetohydrodynamics (MHD). In the case of liquid metals or semiconductor melts, this control method is already in productive use on an industrial scale. The inherent nature of the electromagnetic or Lorentz force allows for a completely contactless influence, which is especially useful in the case of metal casting and, generally, the handling of hot and chemically aggressive melts. To quote Shercliff [6]: "MHD has a peculiar attraction for aerodynamicists and mechanical engineers; instead of being confined to pushing at the edges of fluid streams, they are enabled by MHD to grab the fluid in midstream!". However, experimental results on the use of Lorentz forces in fluids of low conductivity, and even more in aerodynamic applications, are somewhat scarce, though first musings date back to the 1950's, e.g. [7,8]. Experimental evidence of successful separation postponement on a half cylinder in an electrolyte flow has been given in 1962 [9]. A few investigations on related topics have been published in the 1960's e.g. [10–12], but the activities declined afterwards. A renewed interest in the use of Lorentz forces to control the flow of electrolytes arose in the 1990's. The main body of the corresponding research, among several others [13–15], were aimed at drag reduction in turbulent boundary layers. Successful electromagnetic control of the flow around a circular cylinder at low Reynolds numbers has been experimentally demonstrated by [16] and [17]. Numerical treatment of this generic problem can be found, e.g., in [18].

The present paper aims to extend the experimental work on separation control at hydrofoils described in [19] to the application of time periodic Lorentz forces. In [19] the effect of a steady wall parallel Lorentz force on the suction side of symmetric hydrofoils has been investigated. Main flow features as well as governing parameters and scaling relations are discussed. Possible practical applications are, e.g., improved steering rudders and stabilizer fins for marine vessels. Obviously, power consumption is of major concern for such devices, what renders the advertised efficiency increase for periodic excitation [5] highly attractive. This is especially true for the intrinsically low efficiency of direct electromagnetic actuation with weak magnetic fields in low conducting fluids, see e.g. [20], [21] and [22]. On the other hand, the Lorentz force is a direct and easily controllable source of momentum, what makes it an interesting tool for basic research on oscillatory forcing of separated flows.

2 Principle and Parameters

An electromagnetic body force $\mathbf{F}$ results from the vector product of the current density $\mathbf{j}$ and the magnetic induction $\mathbf{B}$

$$\mathbf{F} = \mathbf{j} \times \mathbf{B}. \tag{1}$$

The current density is given by Ohm's law

$$\mathbf{j} = \sigma(\mathbf{E} + \mathbf{u} \times \mathbf{B}), \tag{2}$$

where $\mathbf{E}$ denotes the electric field, $\mathbf{u}$ the velocity, and σ the electrical conductivity, respectively. If the fluid is a liquid metal or semiconductor melt of high electrical conductivity, a fully contactless control of the melt is possible solely by application of a magnetic field. Unlike liquid metals, electrolytes, such as seawater, exhibit only a low electrical conductivity in the order of 10 S/m. As a result, the currents originating from the $(\mathbf{u} \times \mathbf{B})$–term in equation (2) are generally very low, even for magnetic fields of several Tesla. Consequently, the Lorentz force (1) due to these currents is negligible. In order to obtain current densities large enough for flow control purposes it is therefore necessary to apply an electric field of magnitude E_0 with $E_0/(U_\infty B_0) \gg 1$, where U_∞ denotes the freestream velocity. This implies that the force density distribution can be determined independently of the flow field. Note that for the purpose of a energetically efficient drag reduction this statement is not true as has been shown in [20]. Any energetically attractive electromagnetic drag reduction requires to work in a regime where the externally applied currents are of the same order as those originating from the $(\mathbf{u} \times \mathbf{B})$–term. As such a regime requires magnetic fields of several Tesla, however, both from a practical as well as a methodical point of view it is worth to consider at first the decoupled case of a dominating externally applied electric current.

In principle, almost any Lorentz force distribution may be obtained by a suitable combination of electric and magnetic fields. Indeed, if one is able to determine an optimal force distribution for a given flow control problem, it should be possible to solve the inverse problem for the electric and magnetic field configurations. However, in practice certain limitations do exist, e.g. integrating the electrodes and magnets into the given shape of a body. Especially this constraint enforces a decay of the Lorentz force density with the wall distance. Several force configurations have already been investigated with respect to drag reduction of turbulent boundary layers: wall normal Lorentz forces [13], wall parallel forces in spanwise direction [21] and wall parallel forces in streamwise direction [14,19]. The latter configuration is considered in the present paper. The sketch in the left part of *figure 1* shows a stripwise

arrangement of flush mounted electrodes and permanent magnets capable of generating a wall parallel Lorentz force. Such configuration has been proposed by [10] in order to prevent boundary layer transition. Similar configurations are proposed in [12] and [23], with the patent [12] claiming among other things the use for separation suppression and lift increase. Apart from end effects, both electric and magnetic fields possess only components in wall normal (y) and spanwise (z) direction. Consequently (see equation (1)), the Lorentz force has only a streamwise (x) component. Near the plate surface, strong spanwise variations of the force density appear [19], which are caused by singularities of the equations for both magnetic and electric fields at the corners of the permanent magnets and electrodes, respectively. However, these inhomogeneities rapidly decrease with increasing wall distance. Averaged over z, the mean force density shows an exponential decay with increasing wall distance and can be written [24] as

$$F = \frac{\pi}{8} j_0 M_0 e^{-\frac{\pi}{a}y}, \tag{3}$$

with M_0 denoting the magnetization of the permanent magnets and j_0 the applied current density σE_0, respectively. The magnetic induction in wall normal direction at the surface of the magnetic poles B_0 can be calculated from the geometry of the magnets and their magnetization M_0. For magnets infinitely extended in $(-y)$-direction, $B_0 = M_0/2$ applies [24]. Electrodes and magnets have the same width a, a condition maximizing the attainable force density [25].

As can be seen from the Navier–Stokes equations for incompressible flow

$$\frac{\partial \mathbf{u}}{\partial t} + (\mathbf{u} \cdot \nabla)\mathbf{u} = -\frac{\nabla p}{\rho} + \nu \nabla^2 \mathbf{u} + \frac{\mathbf{F}}{\rho}, \tag{4}$$

the electromagnetic force density acts as a momentum source for the flow. In equation (4), t denotes time, p the pressure, ρ the density and ν the kinematic viscosity of the fluid, respectively. Experimental confirmation of the accelerating effect of a wall parallel Lorentz force on a flat plate boundary layer can be found in [14] and [26]. Depending on the force strength, even a distinct wall jet can be established. It may be concluded that stationary Lorentz forces of this kind will have a similar effect on the separated flow over an airfoil, as blowing on the suction side. Indeed, it has been shown in [19] that both methods are comparable even in a quantitative sense. It turned out that a momentum coefficient defined in analogy to that used to describe the effect of a jet [27]

$$c_\mu = \frac{1}{2} \cdot \frac{a j_0 B_0}{\rho U_\infty^2} \cdot \frac{x_e - x_s}{c}, \tag{5}$$

correlates the data fairly well and makes them comparable to those obtained by alternative control methods. c_μ links the total momentum injected into the flow by the Lorentz force to the dynamic pressure. The actuator extends over the length x_e–x_s of the chord c and the full spanwidth.

In order to apply time-dependent forces, the same setup as sketched in the left part of *figure 1* can be used, with the only difference of using alternating currents to feed the electrodes. The corresponding arrangement of the actuator on a symmetric foil is shown in the right part of *figure 1*. Since periodic excitation has proven to be most effective directly at the leading edge [28], actuation should be concentrated there. With the excitation frequency f_e a forcing Strouhal number can be defined as follows

$$St_e = \frac{f_e c}{U_\infty}. \tag{6}$$

The majority of current papers on flow control by oscillatory injection of momentum uses the effective momentum coefficient to describe the forcing level. Its appropriate definition for the case considered here is

$$c'_\mu = \frac{1}{2} \cdot \frac{aB_0}{\rho U_\infty^2} \cdot \frac{x_e - x_s}{c} \cdot \sqrt{\frac{1}{T} \int_0^T j(t)^2 \, dt}, \tag{7}$$

where $j(t)$ denotes the time-dependent applied current density and T is the period of oscillation.

There are several distinct features of the Lorentz force actuator: it does not require calibration since by its nature as a body force momentum is directly generated in the fluid; its frequency response is practically unlimited, virtually any excitation wave form might be realized by feeding the electrodes with an appropriate current. On the other hand, the efficiency of momentum generation by weak magnetic and strong electric fields is generally small, since Joule losses dominate in electrically low conducting fluids.

3 Experimental Setup

The experiments were carried out in the electrolyte tunnel shown in *figure 2*. This tunnel is made from stainless steel, impeller and pump housing consist of plastic. These materials have been chosen in order to avoid possible corrosion problems due to the electrolyte filling. The test section is a 1.2 m long rectangular duct with 0.3 m $\times$ 0.4 m cross section. It is preceded by a nozzle with a contraction ratio of 4.2:1. In the nozzle, the cross section is

transformed from a circular to a rectangular shape. Upstream of the nozzle two polyethylene honeycombs are followed by four stainless steel screens of decreasing mesh width. In front of the honeycombs, a filter pad is mounted in order to absorb impurities from the electrolyte solution. All four elbows of the channel are equipped with turning vanes. The axial pump is driven by a frequency controlled asynchronous motor of 15 kW electrical power allowing for a maximum velocity of 5 m/s inside the test section. In the velocity range $U_\infty \lesssim 1.2$ m/s used in the experiments described here, the turbulence level is $Tu \lesssim 0.7\%$. A 0.25 molar NaOH solution has been used as electrolyte.

Forces on the hydrofoil have been measured by a 5 component strain gage balance. This balance has been designed by the Dresden Technical University for maximum lift and drag values of 1 kN each. Due to the electronically noisy environment generated by the frequency converter of the pump, special care had to be taken in aquiring and transferring the force balance signals. The Wheatstone bridges of the balance are powered by accumulators. 16 bit Analog/Digital converters, powered as well by accumulators, digitize the bridge readouts and transfer them for storage to a PC by optical fibres.

A NACA 0015 foil with chord length $c = 160$ mm and a span width of 240 mm has been chosen for the experiments since its characteristics have been thoroughly investigated by a number of researchers and data for leading edge excitation by oscillatory blowing and suction are available [4]. The actuator extends from the leading edge ($x_s = 0$) to $x_e = 15$ mm, i.e. to approximately 9% of the chord. Magnets as well as electrodes have been machined by an Electrical Discharge Machine (EDM) in such a way that their outer shape is exactly that of the foil. Both magnets and electrodes have a width of $a = 5$ mm. While the magnets are made from NdFeB, the electrodes consist of titanium with the active surface covered by a 10 μm thick layer of platinium. To prevent the corrosion of the magnets, they where coated by a 14 μm Parylene C film. After fabrication and assembling of the system of electrodes and magnets, the NACA 0015 was cast in an epoxy–based polymer in a two-piece mold. This mold has been machined from aluminium using the EDM. Finally, the foil has been painted by a two component epoxy finish. Due to slight offsets between magnets and electrodes, a maximum roughness of 100 μm occurs in the actuator region. Unlike the stainless steel electrodes used in [19], the platinium covered titanium electrodes did not suffer from surface degradation due to corrosion. Reference measuremets of the lift–drag polar without forcing before and after the experiments show an excellent reproducability.

End plates were mounted on the NACA 0015 to minimize end effects. They were made from 3 mm thick PMMA. Their edges are parallel to the chord and form half circles of 45 mm radius at the leading and trailing edge of the foil. A photograph of the NACA 0015 equipped with end plates and mounted on the force balance is shown in the left part of *figure 3*. The right part of this

figure gives measured values of magnetic induction in wall normal direction (B_0) along the magnet surface. The mean value evaluates to $B_0 = 0.33$ T.

A high power amplifier FM 1295 from FM Elektronik Berlin has been used to feed the electrodes. It was driven by a frequency generator 33120A from Agilent. The frequency generator operated controlled by a PC, the electrode current was monitored by means of a shunt and recorded in parallel to the force balance values.

4 Flow visualization

To provide a visual impression of the Lorentz force action on a separated flow, an inclined flat plate equipped with magnets and electrodes has been installed in a smaller electrolyte channel. This channel is driven by a centrifugal pump. The test section with a free surface is 1 m long and has a 0.2 m $\times$ 0.2 m cross section, for more details we refer to [29]. As the larger tunnel, the channel was filled with a 0.25 molar NaOH solution.

Figure 4 shows hydrogen bubble visualizations of the flow around an 15°inclined flat plate. Directly behind the leading edge of the 130 mm long plate the actuator is mounted. It consists of $x_e = 10$ mm long and $a = 10$ mm wide magnets and electrodes. Endplates are fixed on both sides of the plate. The unforced flow (*figure 4a*) at a chord length Reynolds number $Re = 1.4 \times 10^4$ is completely separated, the shear layer originating at the leading edge of the plate shows the typical Kelvin–Helmholtz vortices. A sinusoidal forcing with $St_e = 1.4$ and $c'_\mu = 4.4\%$ (*figure 4b*) reattaches the flow to the plate in an averaged sense. Two vortices move along the plate contour, quite similar to those detectable in figure 1.3 of [30]. The gas bubbles leaving the plate at the trailing edge are a consequence of electrolysis due to the electric current at the electrodes. Note that the relatively large bubbles seen in *figure 4* are a peculiarity of the top down arrangement of the plate, chosen in order to minimize distortion of the flow visualization. Originally small electrolytic bubbles agglomerate below the plate and form the larger ones seen in the photographs. During the force measurements, the electrolytic bubbles were allowed to enter the free stream directly and acted merely as flow tracers. Keeping the excitation frequency constant, but increasing the effective momentum coefficient to $c'_\mu = 8.9\%$ (*figure 4c*) results in smaller vortices with the same distance as before. The region of obviously attached flow between them widens. An increase of the forcing frequency to $St_e = 3.0$ under constant momentum coefficient ($c'_\mu = 8.9\%$, *figure 4d*) changes the number of vortices moving along the plate to three. Still the flow is attached in an averaged sense. This picture changes under further increase of the forcing frequency to $St_e = 5.9$ (*figure 4e*). Now discrete vortices are no longer detectable, instead beyond the plate a region of

separated flow is visible. However, its extent is smaller than in the case of the unforced flow. With even further increased excitation frequency ($St_e = 11.8$, *figure 4f*) the region of separated flow grows. The picture is now similar to the unforced flow, except that the shear layer does not exhibit any regular structures under these forcing conditions. Note that the forcing amplitude is still the same with $c'_\mu = 8.9\%$, i.e. it is clearly to be seen that the forcing effect depends strongly on the excitation frequency.

Compared to the experiments reported in the next section, the forcing amplitude here is quite large. On one hand, this is an expected result. Greenblatt and Wygnanski [31] report on experiments to enhance airfoil performance by periodic excitation at low Reynolds numbers. They found that in order to achieve the same lift gain at $Re = 3 \times 10^4$ a four times larger momentum coefficient had to be applied compared to $Re = 5 \times 10^4$. However, looking at the numerical values reveals that they are still by four ($c'_\mu = 4.4\%$) to eight ($c'_\mu = 8.9\%$) times smaller than those applied here. With a stationary force in streamwise direction and a momentum coefficient of $c_\mu = 8.9\%$, the flow can be reattached as well, but this is not the case for $c_\mu = 4.4\%$.

Although the frequency dependence of the flow evolution is consistent with that expected from an excited mixing layer (see e.g. [4]), under the above considerations it seems not appropriate to interpret *figure 4* only in this sense. Instead, a quasi stationary approach might be as well taken into account, regarding the fact that a stationary force of comparable strength is able to reattach the flow. A characteristic time scale of the global flow is given by c/U_∞. If the forcing is strong enough to reattach the flow under steady conditions, it will do so as well if the period of forcing f_e^{-1} is in the order of c/U_∞. When the force points upstream, a vortex is formed. For higher f_e, corresponding e.g. to $St_e = 11.8$, the global flow is no longer able to react to the forcing.

5 Force measurements

In the following, direct force measurements will be presented for different excitation conditions and Reynolds numbers. Lift and drag are given in uncorrected values of the section lift

$$C_L = \frac{F_L}{\frac{\varrho}{2} U_\infty^2 cs} \tag{8}$$

and drag

$$C_D = \frac{F_D}{\frac{\rho}{2} U_\infty^2 cs} \tag{9}$$

coefficients. As usual, the force values are non-dimensionalized by the dynamic pressure and the foils surface. Every data point represents an average of 16384 samples recorded with a 1 kHz sampling frequency. Care has been taken to exclude transient phenomena from the sampling interval. Following the convention used by Wygnanski and co–workers (see e.g. [4]), momentum coefficients are quoted in percentage terms for convenience.

5.1 Lift and drag at constant angle of attack

Figure 5 gives an overview of the forcing effect at various frequencies, momentum coefficients and different angles of attack. At the low Reynolds number of $Re = 5.2 \times 10^4$, the hydrofoil stalls already at the low angle of attack $\alpha = 13°$. At $\alpha = 14°$ the lift coefficient has only half the value of the attached case, indicating abrupt leading edge stall typical for this low Reynolds number range. Baseline values of C_L and C_D are plotted at $St_e = 0$. Excitation with a relatively small amplitude of $c'_\mu = 0.14\%$ is able to restore the lift of the attached flow. It seems as an obvious assumption to interpret this effect as the result of a boundary layer transition triggered by the forcing. This belief is corroborated by the fact that the effect is nearly independent of the excitation frequency. Under excitation, lift and drag coefficient are nearly constant up to $St_e = 50$ (not shown), i.e. in the full range of frequencies investigated. An increase of the momentum coefficient raises the lift coefficient only slightly, but the drag more pronounced. The latter might be caused by an intensified momentum transfer in the boundary layer due to the excitation. If the flow was already attached to the major part of the hydrofoil, the further increase of excitation amplitude would not cause a distinct change in the lift.

At an inclination angle of $\alpha = 17°$ and $Re = 8.0 \times 10^4$, the flow behaviour changes. For momentum coefficients $c'_\mu \leq 0.23\%$, a strong influence of the excitation frequency on lift as well as on drag is detectable. Both reach maximum values at $St_e = 0.75$. The forcing effect decreases relatively rapidly towards higher as well as lower frequencies. The shape of the C_L versus St_e curve is very similar to those observed for oscillatory leading edge blowing on a NACA 63_3–018 [28] and a NACA 0015 [30]. It is a generally accepted conception that this frequency dependency can be explained by the behaviour of the excited shear layer between the freestream and the separated flow, see [4,28]. The shear layer will amplify the imposed disturbances in such a way that mixing and momentum transport between mean flow and separated region are en-

hanced. If the entrainment caused by this process is large enough, the shear layer will reattach to the boundary in a manner similar to the Coanda effect. According to this theory, the most effective forcing occur at a St_e in the order of 1. For momentum coefficients $c'_\mu \geq 0.23\%$, the lift maximum at $St_e = 0.75$ is still present, but much less pronounced. Instead, forcing in the investigated frequency range of $0.25 \leq St_e \leq 50$ is nearly equally effective (frequencies $St_e > 8$ are not plotted). At $c'_\mu = 0.23\%$ itself, the flow regime seems very sensitive to initial conditions, different runs with this parameter exhibit either a strong or a weak dependence of the force coefficients on the excitation frequency. The maximum lift coefficient in the case of a weak frequency influence is larger ($C_L = 1.04$) than in the case where the flow shows a strong dependence on the excitation frequency ($C_L = 0.93$). It may be an admissible hypothesis to attribute the change in the C_L versus St_e curve to a transition between two different flow regimes. At small momentum coefficients, the excitation of the mixing layer seems to dominate the flow, while a stronger forcing seems to be able to completely reattach the boundary layer. In the time resolved force measurements, the forcing frequency is very dominant for $St_e \leq 0.75$ and $c'_\mu \leq 0.23\%$. Though it is still discernible for $c'_\mu \geq 0.23\%$, the rms value relative to the mean lift is about four times smaller than at lower momentum coefficients. While the mean drag is slightly increased for low St_e and low c'_μ compared to the unforced case, it drops by about 30% for $c'_\mu \geq 0.23\%$. The assumption of two different flow regimes is supported by flow visualizations on a Sikorsky SSC–A09 airfoil section at $Re = 2.5 \times 10^5$ reported by McCormick [32]. That author found at post–stall angles of attack for $c'_\mu = 0.5\%$ a flow dominated by large coherent structures, but reattached in an averaged sense. The situation changes for $c'_\mu = 1.5\%$. At that momentum coefficient the smoke visualization shows a fully attached flow without visible coherent structures.

The bottom part of *figure 5* gives lift and drag coefficients for $Re = 5.2 \times 10^4$ and $\alpha = 20°$. At these parameters the hydrofoil is in deep stall. Excitation with momentum coefficients up to $c'_\mu = 1.11\%$ results in an increase of C_L at $St_e = O(1)$. Higher momentum coefficients were not attainable with the present setup. The C_L versus St_e curves exhibit the typical shape found for shear layer excitation. Forcing with $St_e \gtrsim 6$ has practically no effect on the lift. Corresponding to the lift increase, the drag rises at low excitation frequencies ($St_e \lesssim 3$) compared to the unforced case. Such a drag increase has been observed experimentally before by Hsiao [33] and in numerical investigations of Wu et al. [34]. As well, numerical results on separation control by time periodic Lorentz forces by Mutschke and Gerbeth [35] show this effect. According to Hsiao [33] the reason for the drag rise is an increase of the separation bubble size due to the forcing which results in a larger lift, but due to a broadened wake in an increased drag as well. The momentum coefficients given in *figure 5* indicate that the drag reaches a maximum value for a specific c'_μ. For larger momentum coefficients, the drag decreases. The next subsections present a

closer look at this phenomenon.

5.2 Lift and drag versus momentum coefficient including wave form effects

All results presented so far have been achieved with a sinusoidal forcing, i.e., the alternating current used to feed the electrodes had a sinusoidal wave form. One of the main advantages of using Lorentz forces as momentum source consists in an easy access to modify the wave form of the excitation. For this purpose only the feed current has to be modulated accordingly. To achieve the same goal by traditional means requires a considerable effort as described in [36] and [37]. The differences in applying an excitation with a sinusoidal, triangular or rectangular wave form, which are readily available from standard frequency generators, have been examined.

Figure 6 shows C_L and C_D versus the effective momentum coefficient c'_μ defined by equation (7) for $Re = 5.2 \times 10^4$, $\alpha = 20°$ and $St_e = 0.5$ (left) respectively $St_e = 1.5$ (right). As well known, the square root term in equation (7) evaluates to $\hat{j}/\sqrt{3}$ for triangular, $\hat{j}/\sqrt{2}$ for sinusoidal and $\hat{j}$ for rectangular wave forms, where $\hat{j}$ is the peak current density. Under the conditions utilized in *figure 6*, the difference in the wave form apparently does not influence the forcing effect, all measured points arrange to one curve.

As could be inferred from *figure 5*, the forcing with $St_e = 0.5$ is more effective in terms of lift gain than that with $St_e = 1.5$, though the former leads to a larger drag increase. The C_L versus c'_μ plot in *figure 6* shows a kink for both excitation frequencies. This suggests to fit straight lines to the regions with obviously different slopes. These lines have been included into the figure. Their intersection coincides quite well with the maximum in the corresponding C_D versus c'_μ curves. The initial steeper lift increase is therefore coupled to a drag rise, whereas the following weaker enlargement is accompanied by a decreasing drag. Under forcing with lower frequency ($St_e = 0.5$), the drag maximum occurs with $C_D \approx 0.49$ for $c'_\mu \approx 0.61\%$. The corresponding lift coefficient is $C_L \approx 1.08$. At the higher forcing frequency ($St_e = 1.5$), the drag maximum is lower $C_D \approx 0.41$ and occurs earlier at $c'_\mu \approx 0.41\%$. The lift coefficient at this c'_μ amounts to $C_L \approx 0.84$.

Following the reasoning of Hsiao [33] and the explanation and streamlines given by Wu et al. [34] (esp. figs. 23-25 of this reference), size and position of the lifting vortex in the time averaged flow field is influenced by the excitation and can be used to explain the different behaviour. The integral force values given here suggest that at low excitation levels the lifting vortex is moved towards the foil, thereby increasing lift and drag. For larger excitation levels, the size of the mean separated region is more and more reduced, resulting in a

drag decrease and further lift increase. However, without a detailed knowledge of the flow field, the scenario sketched above remains obviously speculative.

In *figure 7* lift and drag coefficient versus the effective momentum coefficient are given for $St_e = 0.5$ (left) and $St_e = 1.5$ (right) like in *figure 6*, but for the larger Reynolds number $Re = 1.06 \times 10^5$. A technical consequence of the increased Reynolds number is the lower maximum momentum coefficient of $c'_\mu \approx 0.34\%$ achievable with the available power supply. In terms of lift gain, excitation at $St_e = 0.5$ is more effective than at $St_e = 1.5$. However, drag increase as well is more pronounced for the smaller excitation frequency. For $St_e = 1.5$, a drag maximum at $c'_\mu \approx 0.12\%$ is still identifiable, though the data are considerably scattered. The lift data are similarly scattered, especially in the region around the supposed kink. Therefore, the intersection of the two fitted lines at $c'_\mu \approx 0.09\%$ and the drag maximum coincide not as well as in *figure 6*. However, clearly both phenomena, drag maximum and lift curve kink, occur at lower c'_μ than at $Re = 5.2 \times 10^4$. The data for $St_e = 0.5$ given in the left column of *figure 7* show a completely different picture. Lift as well as drag increase versus c'_μ differs evidently for excitations with different wave forms. Forcing with triangular waves results in the steepest lift and drag rise with c'_μ, sinus waves have a less pronounced effect, and excitation with a rectangular wave form shows the smallest increase. There is neither a distinct drag maximum nor a discernible kink in the lift versus c'_μ curve visible. This implies not necessarily that such features do not exist at all, possibly the maximum attainable c'_μ is below the critical value.

Figure 8 displays drag and lift coefficient versus excitation frequency for $Re = 1.06 \times 10^5$, $\alpha = 20°$ and a fixed $c'_\mu = 0.2\%$. Generally, the curve shape is similar to that shown in *figure 5* for $Re = 5.2 \times 10^5$ and $\alpha = 20°$. For $St_e \geq 2$, no systematic influence of the excitation wave form on lift and drag appears. Unlike that, around the most efficient frequency of $St_e = 0.75$, the wave form has a very pronounced effect. Consistent with the data from *figure 7* for $St_e = 0.5$, maximum values of lift and drag are obtained applying triangular waves, the maximum values are smaller for sinusoidal forcing and rectangular waves have the least effect.

The lift increment for excitation with the most effective frequency ($St_e = 0.75$) at $\alpha = 20°$ and $Re = 1.06 \times 10^5$ is shown in *figure 9* versus the effective momentum coefficient c'_μ (left) and the peak momentum coefficient $\hat{c}_\mu$ (right). $\hat{c}_\mu$ is the momentum coefficient defined with the peak value of the current density, i.e.

$$\hat{c}_\mu = \frac{1}{2} \cdot \frac{aB_0\hat{j}}{\rho U_\infty^2} \cdot \frac{x_e - x_s}{c}. \tag{10}$$

While the data follow distinct lines when ΔC_L is plotted versus the effective

momentum coefficient, all data collapse fairly well in the ΔC_L versus $\hat{c}_\mu$ plot. That means, around the most effective excitation frequency not the effective, but the peak momentum input determines the attainable lift increase. Even if the validity of this statement will cease for Dirac pulses, it certainly offers attractive prospects for an efficiency increase of periodic excitation arrangements. As can be inferred from *figure 9* the lift increment for $c'_\mu = 0.26\%$ and excitation with a triangular wave form is approximately 70% larger than that reachable using a rectangular wave form.

5.3 Comparison with oscillatory blowing and suction

In the previous sections, electromagnetic excitation has been shown to reproduce the characteristic frequency dependence of separation control by periodic blowing and suction. A comparison of the lift polar for electromagnetic forcing and that measured for oscillatory blowing from the leading edge of a NACA 0015 (figure 22a of [4]) gives *figure 10*. While Reynolds numbers and excitation frequencies differ, $Re = 5.2 \times 10^4$ and $St_e = 0.5$ for electromagnetic excitation and $Re = 1.5 \times 10^5$ and $St_e = 1.1$ for oscillatory blowing, respectively, the attained lift gain is comparable for similar momentum coefficients. The differences in the curves may be caused mainly by the different Re, aspect ratio and blockage. For electromagnetic forcing, already for the small momentum coefficient of $c'_\mu = 0.06\%$, stall is delayed from 13° to 15° due to a boundary layer transition triggered by the excitation. Lift values in the stalled region are only marginally increased as compared to the unforced flow. The picture changes for larger momentum coefficients, for which the abrupt stall tends to become more gentle. C_L is considerably increased in the post stall region, but the maximum lift increases mainly due to higher critical angles of attack. In the pre–stall region, no data have been acquired for the forced flow, but judging from *figure 5*, only a very modest increase would be expected. Somewhat in contrast to this, for oscillatory blowing a lift increase may be found for almost all angles of attack. This effect might be related to the leading–edge discontinuity present at this airfoil, which has a slightly different geometry in the nose region than a real NACA 0015 and was therefore named TAU 0015 by Joslin et al. [38]. The lift polar for a NACA 0012 at $Re = 2.4 \times 10^5$ and $St_e = 1.5$ given in figure 22b of [4] shows no distinct lift increase for angles of attack $\alpha < 8^\circ$.

For shipbuilding applications like rudders and stabilizer fins the lift gain relative to the separated flow is less important, the increase of the maximum attainable lift

$$\Delta C_{Lmax} = C_{Lmax}(c'_\mu) - C_{Lmax}(c'_\mu = 0) \tag{11}$$

in the full range of inclination angles is of primary interest. *Figure 11* shows this quantity versus the momentum coefficient in the Reynolds number range $5.2\times10^4 \leq Re \leq 1.48\times10^5$. For comparison, corresponding data for oscillatoty blowing from figure 23b of [4] obtained on a NACA 0012 foil for $Re = 2.4\times10^5$ and $St_e = 1.5$ and from figure 14 of [32] on a Sikorsky SSC–A09 foil for $Re = 5\times10^5$ and $St_e = 1.3$ have been included. The relatively large scatter of the data obtained for electromagnetic excitation is mainly a Reynolds number effect since in this range of Re laminar separation bubbles are expected to have a pronounced effect on the overall behavior of the flow. Despite these uncertainties, the data for oscillatory blowing show the same trend and fit in quite well regardless the differences in foil shape and Reynolds number.

5.4 Comparison with stationary forcing

The application of periodic momentum to control separated flows is usually expected to result in a comparable gain for a considerably lower expenditure than in case of steady momentum input (see e.g. [5]). In the case of electromagnetic forcing, this expectation is fulfilled if the lift gain for a fixed angle of attack is considered. Although no direct comparison in the frame of the data presented here is possible since steady Lorentz forces have not been applied to the described NACA 0015, data from experiments with a PTL IV hydrofoil are available. They indicate a decrease of the momentum input necessary to recover the lift of a stalled hydrofoil by a factor of $7\ldots17$ compared to steady forcing. *Figure 12* shows the maximum attainable lift gain according to Equation (11) for both steady as well as time periodic Lorentz forces versus the momentum coefficient. Data for steady forcing are taken from [19] and belong to experiments with PTL IV and NACA 0015 hydrofoils in the Reynolds number range $2.9\times10^4 \leq Re \leq 3.7\times10^5$. Again the considerable scatter might be attributed to the Reynolds number range, different foil shapes, blockage and aspect ratios. However, there is certainly no efficiency gain of an order of magnitude for oscillatory excitation. In the case of steady forcing, lift is increased by two mechanisms: 1) reattaching the separated flow and therefore increasing the critical angle, and 2) introducing circulation due to acceleration of the attached suction side flow. Unlike that, no additional circulation in an already attached flow is generated in the case of periodic excitation. A fit of the ΔC_{Lmax} versus c_μ data for steady Lorentz forces given in [19] indicates that the added circulation contributes substantially to ΔC_{Lmax} in the case of the single element hydrofoils considered here. The case might be different for the high lift configurations with blowing over the flaps, and flap shoulder excitation, respectively. Additionally, unlike steady blowing a steady Lorentz force has no detrimental effect for low momentum coefficients.

6 Conclusions

Experimental results on the use of time periodic Lorentz forces to control the suction side flow of a NACA 0015 hydrofoil have been presented for the Reynolds number range $5.2 \times 10^4 \leq Re \leq 1.5 \times 10^5$. Essential features like characteristic efficient excitation frequencies, effective momentum coefficients and resulting lift gain compare well to that found with alternative methods for periodic addition of momentum.

A specific lift increase with respect to the value for the separated flow can be obtained by oscillatory forcing with fractions of the momentum input necessary for steady Lorentz forces. In contrast, an equal increase of the maximum lift gain requires a similar expenditure of momentum for both control methods.

The Lorentz force allows for a great flexibility in providing the time dependency of the forcing. The application of wave forms different from sinusoidal ones has been found to increase the efficiency under certain conditions by up to 70% compared to a sinusoidal forcing. Around the most efficient excitation frequency, not the effective, but the peak value of the applied momentum coefficient seem to determine the attainable lift gain. That offers a potential for a further energetic optimization of the flow control by unsteady Lorentz forces.

Acknowledgements

We thank David Greenblatt and Duane C. McCormick for the friendly permission to use their data and Fei–Bin Hsiao for fruitful discussion. Financial support from Deutsche Forschungsgemeinschaft (DFG) in frame of the Collaborative Research Centre (SFB) 609 is gratefully acknowledged.

References

[1] G. V. Lachmann (Ed.), Boundary Layer and Flow Control, Vol. 2, Pergamon Press, Oxford, 1961.

[2] P. K. Chang, Control of Flow Separation, Hemisphere, Washington, 1976.

[3] M. Gad–el–Hak, Flow Control: Passive, Active, and Reactive Flow Management, Cambridge University Press, 2000.

[4] D. Greenblatt, I. J. Wygnanski, The control of flow separation by periodic excitation, Prog. Aero. Sci. 36 (2000) 487–545.

[5] I. Wygnanski, Boundary layer and flow control by periodic addition of momentum, in: 4^{th} AIAA Shear Flow Control Conference, Snowmass Village, CO, 1997, also as AIAA–97–2117 paper.

[6] J. Shercliff, A Textbook of Magnetohydrodynamics, Pergamon Press, Oxford, 1965.

[7] V. J. Rossow, On flow of electrically conducting fluids over a flat plate in the presence of a transverse magnetic field, Tech. Rep. TN 3971, NACA (1957).

[8] E. L. Resler, W. R. Sears, The prospects for magneto–aerodynamics, J. Aero. Sci. 25 (4) (1958) 235–245.

[9] O. Lielausis, A. Gailitis, R. Dukure, Boundary layer control by means of electromagnetic forces, in: Proc. Int. Conf. on Energy Transfer in Magnetohydrodynamic Flows, Cadarache, France, 1991, pp. 5–9.

[10] A. Gailitis, O. Lielausis, On a possibility to reduce the hydrodynamic resistance of a plate in an electrolyte, Applied Magnetohydrodynamics. Reports of the Physics Institute 12 (1961) 143–146, in Russian.

[11] A. B. Tsinober, A. G. Shtern, On the possibility to increase the stability of the flow in the boundary layer by means of crossed electric and magnetic fields, Magnitnaya Gidrodinamika 3 (2) (1967) 152–154, in Russian.

[12] R. X. Meyer, Magnetohydrodynamic method and apparatus, US Patent 3,360,220 (1967).

[13] D. Nosenchuck, G. Brown, Discrete spatial control of wall shear stress in a turbulent boundary layer, in: R. So, G. Speziale, B. Launder (Eds.), Near–Wall Turbulent Flows, Elsevier, 1993, pp. 689–698.

[14] C. Henoch, J. Stace, Experimental investigation of a salt water turbulent boundary layer modified by an applied streamwise magnetohydrodynamic body force, Phys. Fluids 7 (1995) 1371–1383.

[15] Y. Du, G. E. Karniadakis, Suppressing wall turbulence by means of a transverse traveling wave, Science 288 (2000) 1230–1234.

[16] T. Weier, G. Gerbeth, G. Mutschke, E. Platacis, O. Lielausis, Experiments on cylinder wake stabilization in an electrolyte solution by means of electromagnetic forces localized on the cylinder surface, Experimental Thermal and Fluid Science 16 (1998) 84–91.

[17] S.-J. Kim, C. M. Lee, Investigation of the flow around a circular cylinder under the influence of an electromagnetic force, Exp. Fluids 28 (2000) 252–260.

[18] O. Posdziech, R. Grundmann, Electromagnetic control of seawater flow around circular cylinders, Europ. J. Mechanics/B Fluids 20 (2001) 255–274.

[19] T. Weier, G. Gerbeth, G. Mutschke, O. Lielausis, L. Lammers, Control of flow separation using electromagnetic forces, Flow, Turbulence and Combustion 71 (1–4) (2003) 5–17.

[20] V. I. Shatrov, V. I. Yakovlev, Optimization of the internal source in the problem of MHD flow around a sphere, J. Applied Mechanics and Technical Physics 33 (1992) 334–341.

[21] T. W. Berger, J. Kim, C. Lee, J. Lim, Turbulent boundary layer control utilizing the Lorentz force, Phys. Fluids 12 (3) (2000) 631–649.

[22] K. S. Breuer, J. Park, C. Henoch, Actuation and control of a turbulent channel flow using Lorentz forces, Phys. Fluids 16 (4) (2004) 897–907.

[23] W. A. Rice, Propulsion system, US Patent 2,997,013 (1961).

[24] V. V. Avilov, Electric and magnetic fields for the Riga plate, Tech. rep., FZR, Rossendorf (July 1998).

[25] E. Grinberg, On determination of properties of some potential fields, Applied Magnetohydrodynamics. Reports of the Physics Institute 12 (1961) 147–154.

[26] T. Weier, U. Fey, G. Gerbeth, G. Mutschke, O. Lielausis, E. Platacis, Boundary layer control by means of wall parallel Lorentz forces, Magnetohydrodynamics 37 (1/2) (2001) 177–186.

[27] P. H. Poisson-Quinton, Einige physikalische Betrachtungen über das Ausblasen an Tragflügeln, Jahrbuch der WGL (1956) 29–51.

[28] F.-B. Hsiao, C.-F. Liu, J.-Y. Shyu, Control of wall–separated flow by internal acoustic excitation, AIAA Journal 28 (8) (1990) 1440–1446.

[29] T. Weier, G. Gerbeth, U. Fey, G. Mutschke, O. Posdziech, E. Platacis, O. Lielausis, Some results on electromagnetic control of flow around bodies, in: Int. Symp. on Seawater Drag Reduction, 1998, pp. 229–235.

[30] I. Wygnanski, A. Seifert, The control of separation by periodic oscillations, in: 18^{th} AIAA Aerospace Ground Testing Conference, Colorado–Springs, CO, 1994, also as AIAA–94–2608 paper.

[31] D. Greenblatt, I. J. Wygnanski, Use of periodic excitation to enhance airfoil performance at low Reynolds numbers, J. Aircraft 38 (1) (2001) 190–192.

[32] D. C. McCormick, Boundary layer separation control with directed synthetic jets, in: 38^{th} AIAA Aerospace Sciences Meeting & Exhibit, Reno, NV, 2000, also as AIAA–2000–0519 paper.

[33] F.-B. Hsiao, Private communication (2003).

[34] J.-Z. Wu, X.-Y. Lu, A. G. Denny, M. Fan, J.-M. Wu, Post–stall flow control on an airfoil by local unsteady forcing, J. Fluid Mech. 371 (1998) 21–58.

[35] G. Mutschke, G. Gerbeth, Numerical investigation of separation control with time periodic Lorentz forces., Tech. rep., FZR, Rossendorf (August 2003).

[36] C. Bouras, H. Nagib, F. Durst, U. Heim, Lift and drag control on a lambda wing using leading-edge slot pulsation of various wave forms, Bulletin of the American Physical Society 45 (9) (2000) 30.

[37] F. Durst, U. Heim, B. Ünsal, G. Kullik, Mass flow rate control system for time–dependent laminar and turbulent flow investigations, Meas. Sci. Technol. 14 (2003) 893–902.

[38] R. D. Joslin, L. G. Horta, F.-J. Chen, Transitioning active flow control to applications, in: 30^{th} AIAA Fluid Dynamics Conference, Norfolk, VA, 1999, also as AIAA–99–3575 paper.

List of Figures

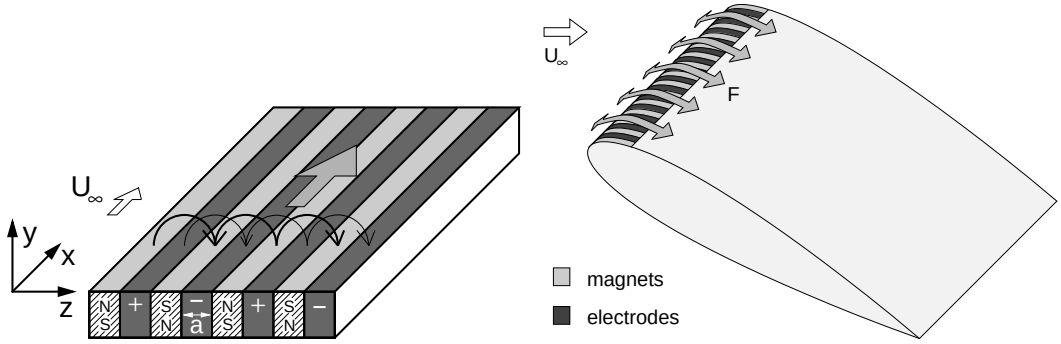

Fig. 1. Configuration of electrodes and permanent magnets to generate a wall–parallel Lorentz force in streamwise direction (left) and application to the hydrofoil (right).

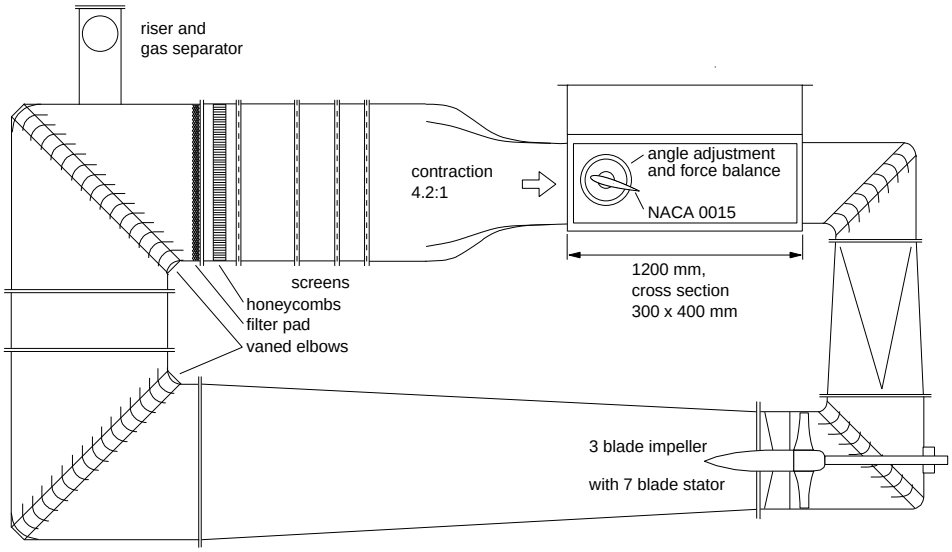

Fig. 2. Electrolyte tunnel at Forschungszentrum Rossendorf.

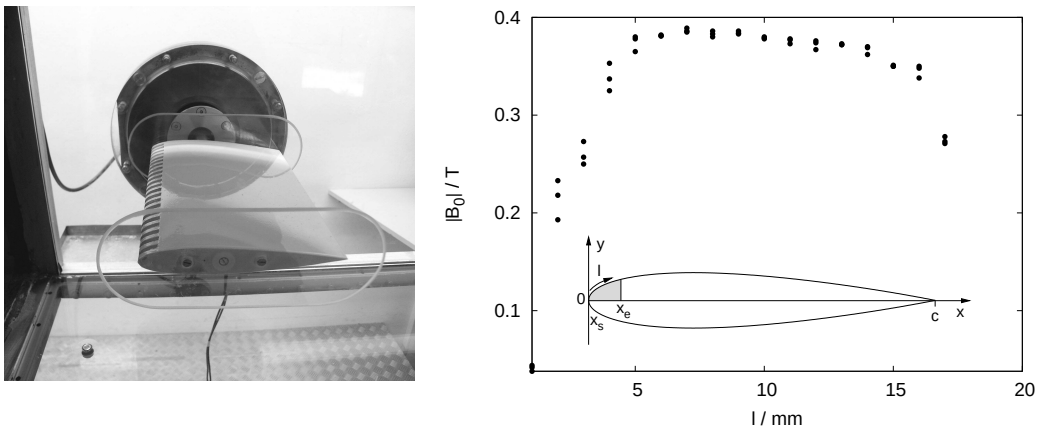

Fig. 3. NACA 0015 with end plates in the test section (left) and magnetic field distribution along the surface of the magnets (right). l denotes here the coordinate along the foil surface.

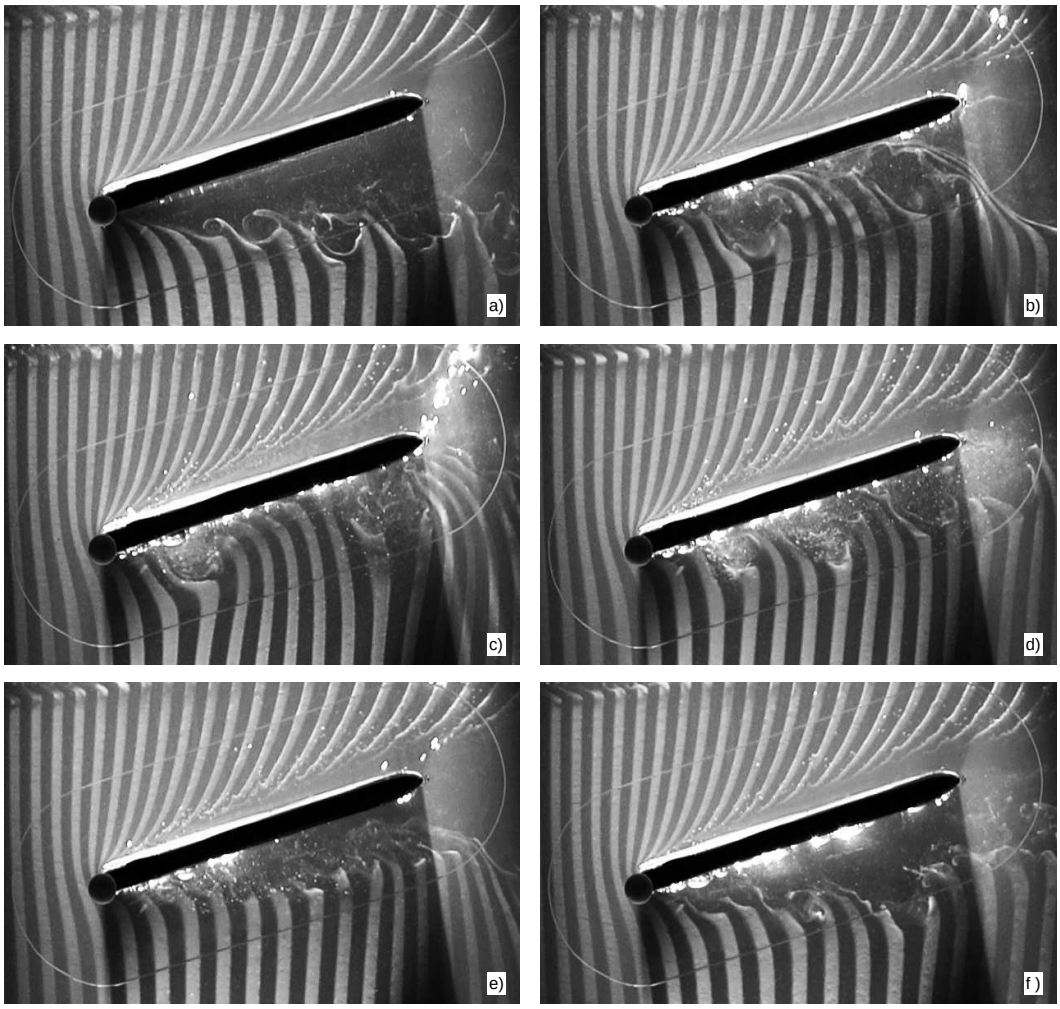

Fig. 4. Excitation of the separated flow at an 15° inclined flat plate at $Re = 1.4 \cdot 10^4$. Forcing at the first 8% chord with a) basic flow; b) $c'_\mu = 4.4\%$, $St_e = 1.4$; c) $c'_\mu = 8.9\%$, $St_e = 1.4$; d) $c'_\mu = 8.9\%$, $St_e = 3.0$; e) $c'_\mu = 8.9\%$, $St_e = 5.9$; f) $c'_\mu = 8.9\%$, $St_e = 11.8$.

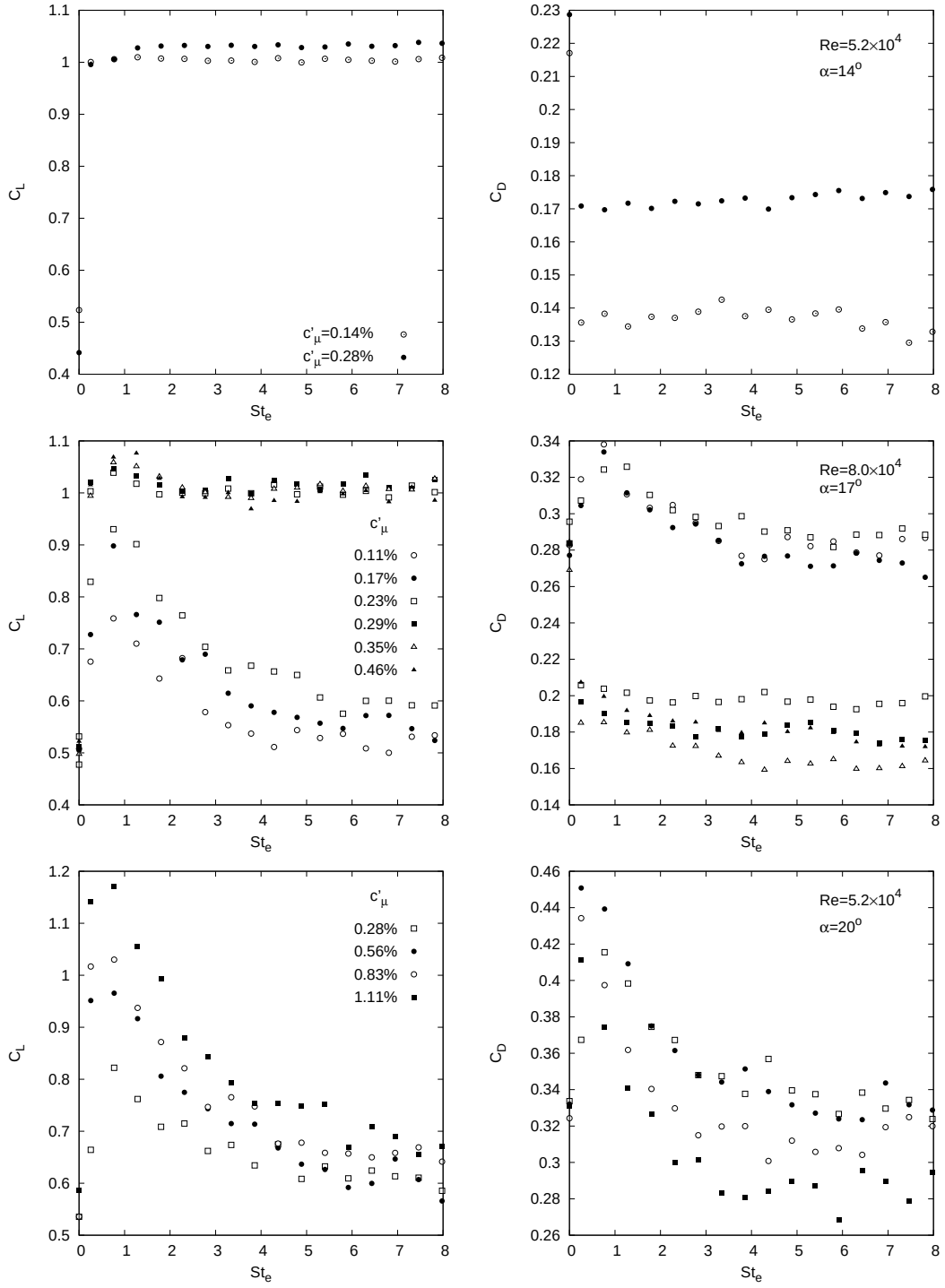

Fig. 5. Influence of the excitation frequency on C_L and C_D at different angles of attack. Top: $\alpha = 14°$, $Re = 5.2 \times 10^4$; middle: $\alpha = 17°$, $Re = 8.0 \times 10^4$; bottom: $\alpha = 20°$, $Re = 5.2 \times 10^4$.

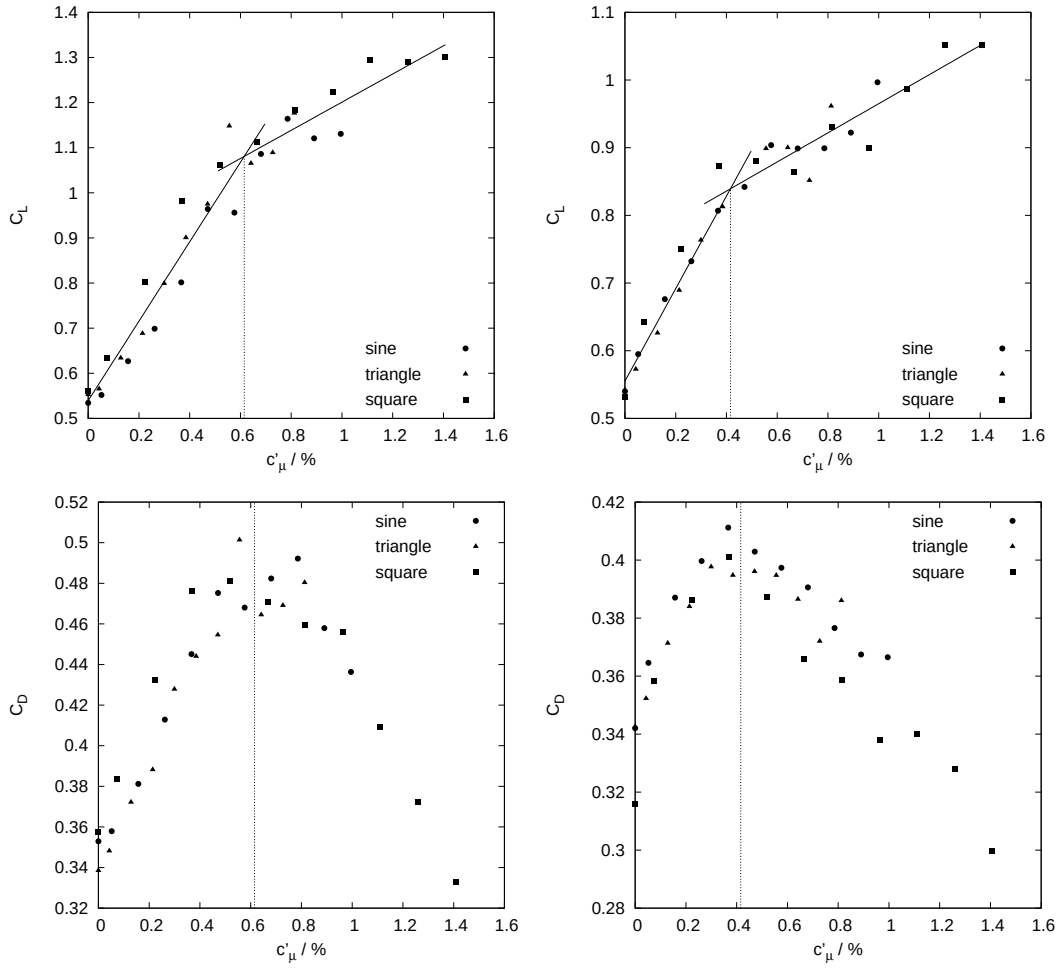

Fig. 6. C_L and C_D versus momentum coefficient for $Re = 5.2 \times 10^4$ and $\alpha = 20°$. Exitation with different waveforms at $St_e = 0.5$ (left) and $St_e = 1.5$ (right).

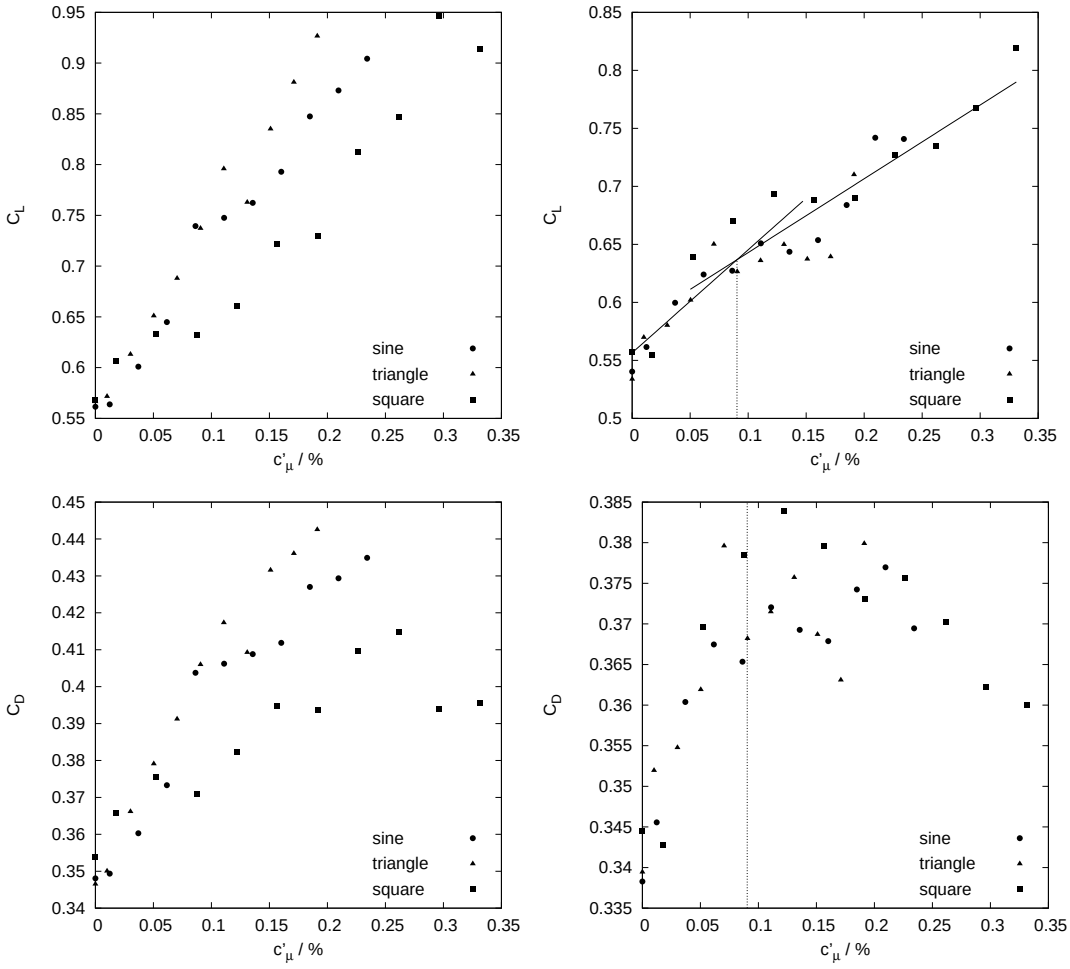

Fig. 7. C_L and C_D versus momentum coefficient for $Re = 1.06 \times 10^5$ and $\alpha = 20°$. Excitation with different waveforms at $St_e = 0.5$ (left) and $St_e = 1.5$ (right).

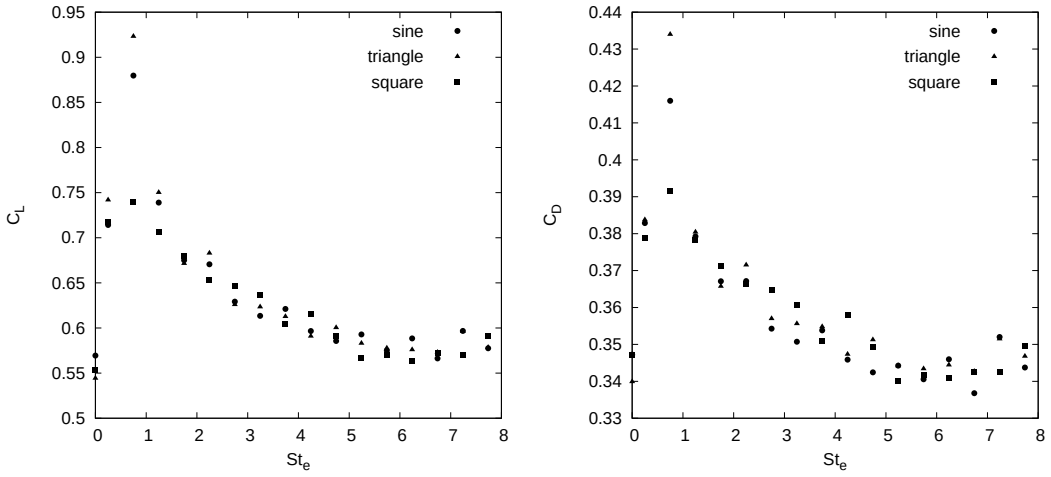

Fig. 8. C_L and C_D versus excitation frequency for different wave forms $Re = 1.06 \times 10^5$, $\alpha = 20°$, $c'_\mu = 0.2\%$.

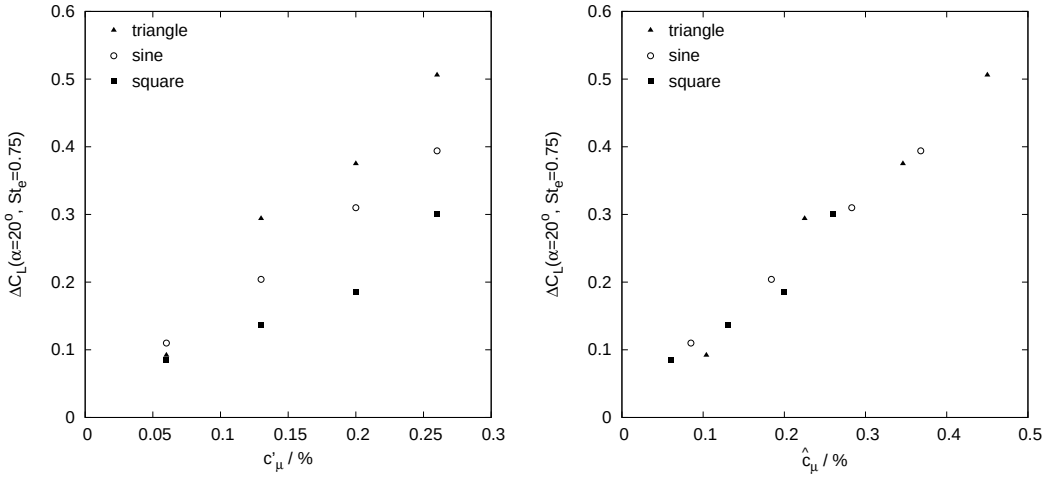

Fig. 9. C_L increase at $Re = 1.06 \times 10^5$, $St_e = 0.75$ and $\alpha = 20^\circ$ versus the efficient (left) and the peak (right) momentum coefficient.

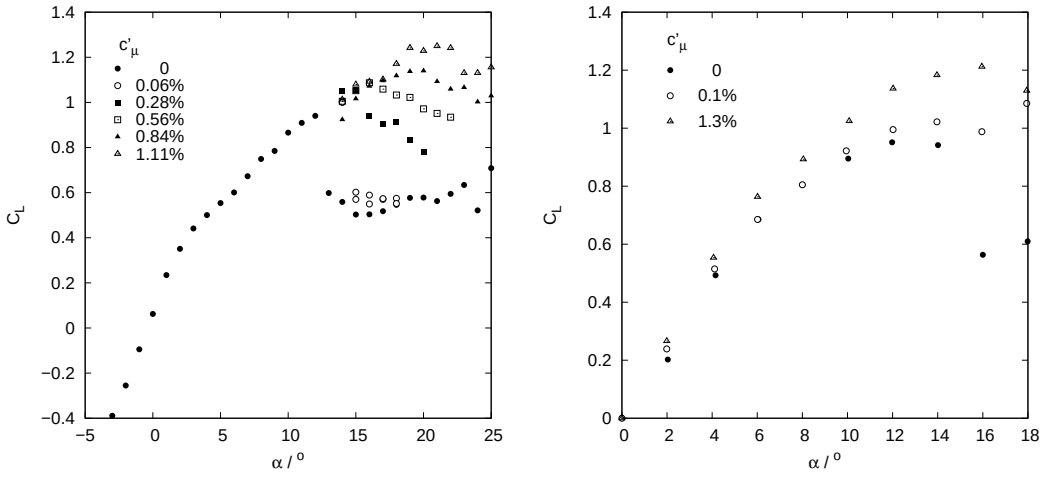

Fig. 10. Electromagnetic excitation at $Re = 5.2 \times 10^4$, $St_e = 0.5$ (left) compared to oscillatory blowing from the leading edge of a NACA 0015 at $Re = 1.5 \times 10^5$, $St_e = 1.1$ (right). With permission from [4].

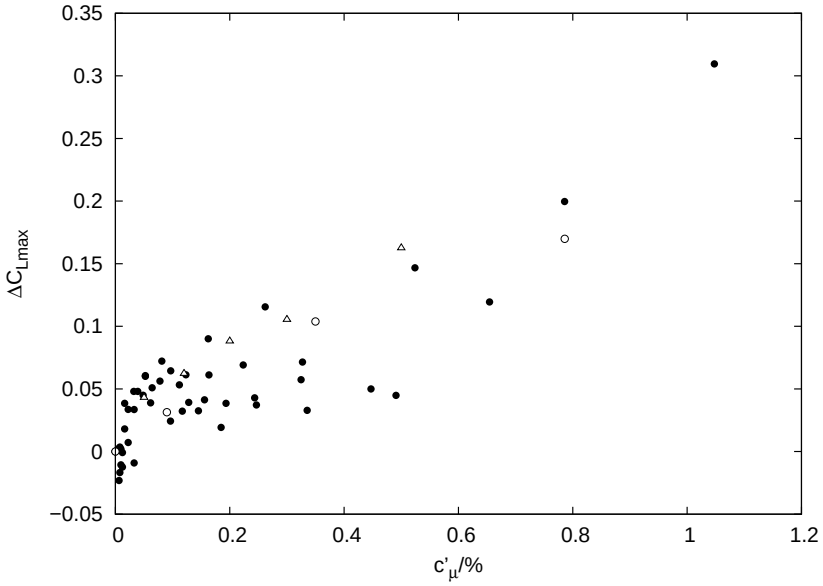

Fig. 11. Maximum lift gain by electromagnetic excitation at $Re = 5.2 \times 10^4 \ldots 1.48 \times 10^5$, $St_e = 0.5$ (filled symbols) compared to oscillatory blowing from the leading edge of a NACA 0012 at $Re = 2.4 \times 10^5$, $St_e = 1.5$ (open circles) and a Sikorsky SSC–A09 at $Re = 5 \times 10^5$, $St_e = 1.3$ (open triangles). With permission from [4] and [32].

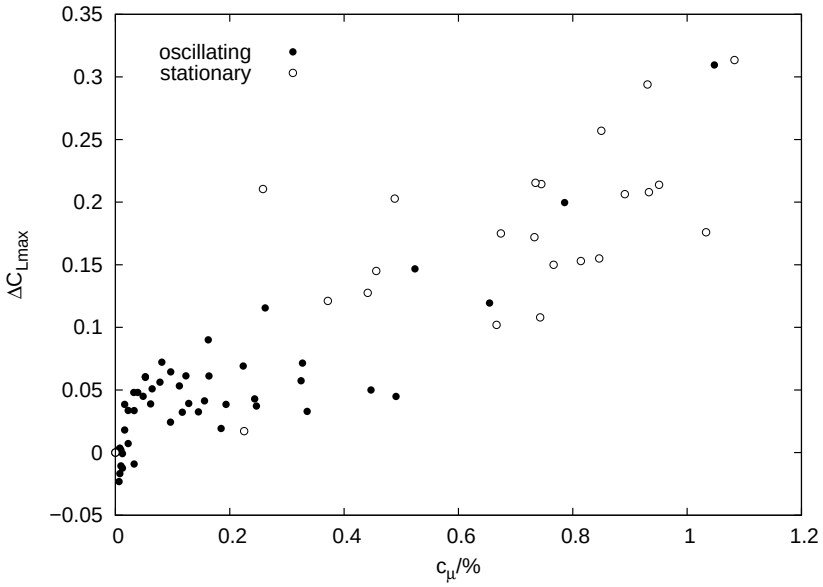

Fig. 12. Maximum lift gain by electromagnetic forces: oscillatory excitation and stationary action compared.